LA-4068-MS

~~CONFIDENTIAL~~   UNCLASSIFIED

C.3

LOS ALAMOS SCIENTIFIC LABORATORY
of the
University of California
LOS ALAMOS • NEW MEXICO

Quarterly Status Report on

Plutonium-238 Space Electric Power

Fuel Development Program (U)

July 1-September 30, 1968

UNCLASSIFIED

~~CONFIDENTIAL~~

UNCLASSIFIED

This LA. . .MS report, the first in a series, presents the status of the Plutonium-238 Space Electric Power Fuel Development Program of Group CMB-11 of LASL.

This report, like other special-purpose documents in the LA. . .MS series, has not been reviewed or verified for accuracy in the interest of prompt distribution.

Distributed December 31, 1968

LA-4068-MS
C-92a, ISOTOPIC SNAP
M-3639 (59th Ed.)

UNCLASSIFIED

LOS ALAMOS SCIENTIFIC LABORATORY
of the
University of California
LOS ALAMOS • NEW MEXICO

Quarterly Status Report on

Plutonium-238 Space Electric Power Fuel Development Program (U)

July 1-September 30, 1968

to

Space Isotopic Fuels and Materials Branch

Space Electric Power Office

Division of Space Nuclear Systems

UNCLASSIFIED

UNCLASSIFIED

PROGRAM 07433

PLUTONIUM-238 SPACE ELECTRIC POWER FUEL DEVELOPMENT

Person in Charge: R. D. Baker

Principal Investigator: J. A. Leary

I. INTRODUCTION

A. Properties of solid solutions and possible advantages

In order to gain some insight into what is meant by a solid solution fuel, it would be helpful to describe its structure.

Consider a simple crystallographic lattice array of plutonium and oxygen atoms. In the case of PuO_2, the plutonium atoms are located in a face-centered cubic a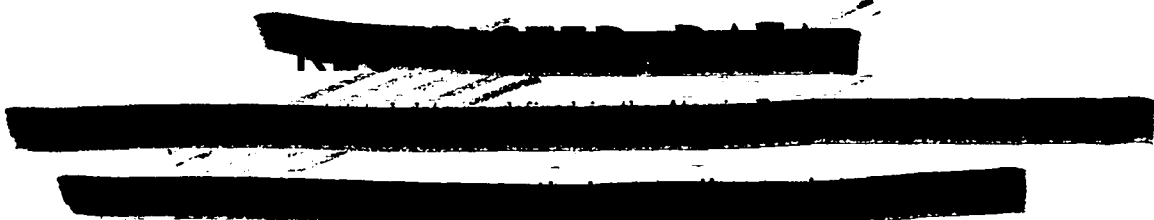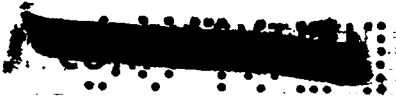rray. A plutonium atom can be removed from the crystal lattice, and its position can be filled by substituting a diluent atom such as zirconium or thorium. This substitution can be continued until a large fraction of the plutonium atoms has been replaced. The diluent atom will be larger or smaller than the plutonium atom, so some expansion or contraction of the crystallographic unit cell will occur. However, as long as the crystal habit remains unchanged, one has a solid solution of the diluent atom oxide in PuO_2. In some systems there is only limited solubility, while in others the solubility is very extensive.

For this application diluents that have very high solubilities were selected. Moreover, the diluents were chosen to enhance the properties of the PuO_2. For example, diluents having oxides that are more stable than PuO_2 were selected so that the resulting solid solution would be more stable than PuO_2. The free energies of formation of these diluents are compared to those of PuO_2 in Table I. The following properties of such solid solutions may be predicted on the basis of known thermodynamic correlations:

1. The thermal stability of the PuO_2 is increased. Thus the tendency for PuO_2 to dissociate or vaporize is reduced. Moreover, the melting point can be increased.

2. The power density of a given fuel body can be varied over a significant range with minimal change in fuel properties.

3. By judicious choice of diluent the reactivity of PuO_2 with water and with container materials can be reduced.

4. The specific radioactivity of a given size

UNCLASSIFIED 3

respirable particle of PuO_2 is reduced.

In addition to these possible advantages, the process for making solid solution fuels is relatively economical. It consists of simply blending unshaped PuO_2 and diluent oxide powders, followed by cold pressing and sintering. It should be noted that it is not necessary to melt the fuel in order to prepare a solid solution; the solution is formed by a solid state diffusion during the sintering process.

B. The overall program

The first task in the program was to conduct an accelerated short-term development phase to provide a technical basis for estimating the performance of $^{238}PuO_2$ solid solution fuels by November, 1968. This included process chemistry development, fabrication development, properties measurements, and theoretical estimates of performance of various fuel compositions and various power densities.

The second task involves follow-on fabrication and properties work with the preferred fuel composition for the purpose of establishing the capability for producing a limited number of large specimens for use as heat sources.

The later tasks in the program are directed towards defining production methods and economics, and to provide assistance to the Commission and its contractors in order to establish a reliable commercial capability.

II. SHORT-TERM ACCELERATED SURVEY

A. Objectives

1. Select fuel composition and power density
2. Develop synthesis and fabrication procedures
3. Prepare small ^{239}Pu pellets and make the following screening measurements:

    A. Crystallography

    B. Microstructure

    C. Chemical composition, purity, and uniformity

    D. Density

    E. Thermal analysis

    F. Preliminary "long term" compatibility at $900^{\circ}C$, and short term overtests.

4. Measure additional properties with ^{238}Pu specimens

    A. Helium migration ($700^{\circ}C$ to $1400^{\circ}C$)

    B. Prepare samples for thermal diffusivity measurements

    C. Prepare samples for sea water solubility measurements

5. Calculate and estimate properties

    A. Thermal conductivity (use thermal diffusivity data, if available)

    B. Long term compatibility

    C. External radiation; the feasibility of using enriched ^{18}O

    D. Radiochemical changes in fuel over lifetime, and their effects

    E. Basic thermodynamic properties

6. Demonstrate fabrication of discs (about 2 in. diam. x 0.5 in. tall) and demonstrate individual disc encapsulation, if required.

7. Additional requirements for SEPO/SNS Safety Evaluation

    A. Arc tunnel tests (pellets)

    B. Impact tests (discs)

    C. Unspecified tests

B. Results and current status

1. Fuel selection: It has not been possible to select a given fuel composition and power density for near term applications. Therefore, three reference power densities (1.7, 3.5, and 4.4 watts/cc) and two diluents (ZrO_2 and ThO_2) are being carried forward in the program.

2. Synthesis and fabrication of properties specimens: The following types of specimens have been fabricated by the process shown in Figure 1: (a) Pellets, 0.254 in. dia x 0.35 in. long with axial hole 0.060 in. dia x 0.080 in. deep; (b) Pellets, as above, except 0.25 in. long; (c) Pellets, as above, without axial hole; (d) Thin wafers, 0.250 in. dia x 0.035 in. thick; (e) Large discs, nominally 2 in. dia x 0.5 in. thick; (f) Same as (e), except 0.25 in. thick.

All of the above specimens have been fabricated with the first reference fuel composition, PuO_2-ZrO_2,*

* The ZrO_2 used in this work contains 4.8 percent by weight CaO stabilizer

4

at a plutonium concentration that corresponds to a power density of 1.7 watts/cc. In addition, compositions equivalent to 3.5 and 4.4 watts/cc have been fabricated. Specimens that have been prepared during this phase of the program are shown in Table II. In addition, the fabrication of large $^{238}PuO_2$-ZrO_2 discs has been started. Typical fabricated specimens are shown in Figures 2, 3, and 4.

Experience has indicated that both the ZrO_2 — and the ThO_2 — diluent fuels can be fabricated directly in any of the reference power densities.

The overall yield of PuO_2 in producing the large discs is 98 percent. Typical fabrication conditions are as follows:

Powder particle size(mmd)	1.5-2.5μ
Pressing pressure	7.5-20 tsi
(with preslugging; large discs pressed with paraffin binder)	
Sintering Atmosphere	CO_2
Sintering Time	6 hr
Sintering Temperature	1625°C

3. Screening measurements:

A. **Crystallography:** All of the reference fuel systems have been shown to be face-centered cubic (fluorite) structure over the complete range of composition, as indicated in Figure 5. The uniform change in lattice parameter with PuO_2 concentration shown for the $ZrO_2|CaO|$, ThO_2, and CeO_2 diluents indicate that these form complete solid solution systems with PuO_2. On the other hand, there is a limit in the solubility of PuO_2 in unstabilized ZrO_2; the fcc solid solution region extends only to 77 mole percent ZrO_2 (at room temperature), and monoclinic ZrO_2 is in equilibrium with the saturated fcc structure at higher ZrO_2 concentrations.

B. **Microstructure:** Typical microstructures are shown in Figures 6, 7, and 8. The $^{239}PuO_2$ and $^{238}PuO_2$ structures shown in Figure 6 are typical of those previously experienced at this Laboratory.[1] The PuO_2-ZrO_2 structures reflect the Si, Al, and Fe impurities that are present in commercial grade ZrO_2 (see next section). These elements appear in the grey grain boundary phases. As the effects of such impurity phases are not yet known, no attempt has been made to eliminate them from the starting ZrO_2 powder. The

PuO_2-ThO_2 microstructure shown in Figure 8 does not show any evidence of impurity phases.

Alpha radioautographs of the 1.7 and 4.4 watts/cc compositions indicate uniform power densities, as shown in Figure 9.

C. **Chemical Composition:** The chemical compositions of the solid solution materials are essentially identical to those of the starting powders. A small amount of iron is picked up in powder milling steps. Chemical purities are shown in Table III.

D. **Density:** During the accelerated phase of the program the standard ceramic engineering relationships (density as a function of pressing pressures, sintering temperature, etc.) were not studied. Instead the desired densities were obtained by pressing and sintering the specimens under conditions that were generated in earlier work with PuO_2 powders.[1] Densities ranging from 70 percent to 96 percent of theoretical have been produced.

E. **Thermal Analysis:** The melting curves for PuO_2-ThO_2 and PuO_2-ZrO_2 (unstabilized) appear in the literature, and are reproduced in Figure 10. Also shown in this figure are melting points obtained by high temperature differential thermal analysis of the solid solution fuels. When the 39 m/o PuO_2-ZrO_2 (1.7 watt/cc) composition was cycled thermally to the melting point, no transitions were indicated until melting occurred at 2400°C (4350°F). The 40 m/o PuO_2-ThO_2 did not display any transition up to the melting point. The solidus temperature was 2725°C (4950°F); the liquidus temperature was 2925°C (5300°F).

F. **Compatibility:** In general, the compatibility of pure solid solution oxides can be estimated quite well from results obtained with PuO_2, ZrO_2, and ThO_2. Because of the known degree of compatibility between PuO_2 and Mo, TZM (99.4% Mo, 0.5% Ti, 0.08% Zr, 0.02% C) alloy was chosen as the possible cladding material to be first investigated. The maximum safe long-term operating temperature for the furnaces immediately available is 1000°C, so 900°C was chosen as a suitable temperature for investigation. Inconel 718 was selected as a material suitable for containing

5

materials under test. One Inconel 718 test capsule (SCC-1) was loaded with TZM and tested for 355 hours at 900°C. Metallographic examinations subsequent to this exposure revealed no reaction, therefore the primary test array has been standardized as follows:

a. The containment tube is of Inconel 718 (nominal analysis Ni-53, Cr-18, Fe-18.5, Nb + Ta-5.0, Mo-3.2, Ti-0.9, Al-0.4, Si-0.3), 0.350 in. O.D., 0.020 in. wall, approximately 2-1/2 in. long; ends are welded cups.

b. An inner liner of 0.002 in. Mo sheet is used (in all TZM tests) to prevent contact between test pellets and side walls. A strip of 0.002 in. Ni is spot-welded across the bottom of the Mo tube as a loading aid.

c. A coil spring wound from 0.030 in. Mo wire is utilized to provide initial contact and to prevent movement during handling.

These arrangements are illustrated in Fig. 11.

Five capsules have been loaded, as listed in Table IV.

Capsule SCC-2 was removed from test after 744 hours (3 900°C). After cooling, the end of the capsule was removed and the contents were vacuum impregnated with a mounting epoxy (EPON 815). The capsule was then mounted in the same epoxy and nearly half its diameter was removed by hand grinding. The mounted capsule was prepared metallographically and the TZM-ceramic interfaces were examined and photographed.

Figure 12 shows the sectioned capsule and the stacking order of the compatibility test cylinders.

Figure 13 shows photomicrographs of the three TZM-ceramic interfaces. Examinations revealed no evidence of reaction between the materials.

Additional compatibility tests are scheduled wherein other potential clads may be evaluated. Orders have been placed for T-111, T-222, W-25 Re, Pt-20 Rh, and Pt-40 Rh. High temperature compatibility studies also are scheduled.

4. Additional properties with ^{238}Pu specimens:

A. Helium Migration: The 0.25 in. dia x 0.25 in. tall pellets that have been put in storage to accumulate He from alpha decay are shown in Table V.

B. Thermal Diffusivity: The four wafers of ^{238}PuO$_2$-ZrO$_2$ solid solution material shown in Table VI have been fabricated and shipped to Battelle Pacific Northwest Laboratory for thermal diffusivity measurements. In addition, two 100% ^{238}PuO$_2$ and ^{238}PuO$_2$-ThO$_2$ specimens are being prepared.

C. Sea Water Solubility: The sixteen samples listed in Table VII have been fabricated and shipped to the Naval Radiological Defense Laboratory at San Francisco for solubility tests. One pellet of each power density was equipped with a 0.060 in. dia blind axial hole for thermocouple insertion.

D. Solubility in Dilute Acid: The solution rates of ^{238}PuO$_2$-ThO$_2$ (1.7 watts/cc) and plasma torch microspheres were compared in the following experiment. Ten milligrams of ^{238}PuO$_2$ microspheres and one 0.25 in. dia by 0.25 in. tall ^{238}PuO$_2$-ThO$_2$ solid solution pellet were rinsed with water, then each was placed in contact with 200 ml of 0.1 N H$_2$SO$_4$. After stirring continuously, a portion of each acid solution was assayed for plutonium. The solubility rate was 1.6 mg Pu/hr/g sample for the microspheres, and 0.0023 mg Pu/hr/g sample for the solid solution fuel. Thus the rate of solution of microspheres was 700 times that of the solid solution, on a sample weight (not on a wattage) basis. If this were referred to the relative surface areas of the two fuel forms, this would correspond to 6.2×10^{-4} mg Pu/sq. mm/hr for the microspheres, and 0.25×10^{-4} mg Pu/sq. mm/hr for the solid solution. On this basis, the microsphere solution rate was 25 times that of the solid solution form.

5. Calculated and estimated properties: Data sheets have been prepared for the PuO$_2$-ZrO$_2$ and the PuO$_2$-ThO$_2$ fuels (see appendix).

A. Thermal Conductivity: The thermal conductivity for the 1.7 and 3.5 watt/cc compositions have been estimated from literature citations of the thermal conductivities of UO$_2$, PuO$_2$, ZrO$_2$, UO$_2$-ZrO$_2$ solid solutions, and UO$_2$-ThO$_2$ solid solutions. These conductivities were used to calculate the radial thermal gradient in a stack of 2.3 inch diameter discs.

6

Maximum gradients were 100° and 200°C for the 1.7 and 3.5 watts/cc ThO_2 diluent, respectively. If the ZrO_2 diluent were used, the gradients would be 112° and 300°C, respectively. Thus higher conductivity and a higher melting point is possible in the PuO_2-ThO_2 system.

B. External Radiation; The Feasibility of Using Enriched ^{16}O: When ^{238}Pu metal is oxidized to $^{238}PuO_2$ in air, the increase in neutron emission rate is 9700 n/sec - g Pu. This is caused by the reactions $^{17}O\,(\alpha, n)\,Ne^{20}$ and $^{18}O\,(\alpha, n)\,Ne^{21}$. These reactions also increase the photon emission rates. These increases can be eliminated if pure ^{16}O is used to prepare $^{238}PuO_2{}^{16}$. However, the basic emission rate (from spontaneous fission and neutron self-multiplication) of about 3000 n/sec - g Pu cannot be reduced. Experience has shown that $^{238}PuO_2$ powders received at this Laboratory can emit 45,000 - 100,000 n/sec - gPu, because of (α, n) reactions on light element impurities.[4]

Conventional ^{238}Pu also contains about 1.2 ppm ^{236}Pu, which decays to ^{212}Pb and ^{208}Tl daughters that produce intense penetrating gamma radiation. Dose rate contributions can be calculated directly once the system geometry is defined.

C. Radiochemical Changes in Fuel: The major change in the conversion of ^{238}Pu to ^{234}U by alpha decay. Since the UO_2-ZrO_2-CaO system is a solid solution system,[5] and since UO_2-PuO_2 also form a continuous series of solid solutions, the ^{234}U should also be in solution as it is produced. While lattice vacancies and new interstitial locations occur at room temperature because of alpha decay, these dislocations anneal out at higher temperature in $^{238}PuO_2$.[6] Chemical changes caused by decay of other isotopes such as ^{236}Pu should be insignificant. The effect of He accumulation in the fuel lattice is not predictable at this time for any $^{238}PuO_2$ fuel forms. However, experimental work is in progress.

D. Basic Thermodynamic Properties: (See Data Sheets in Appendix)

6. Demonstrate Fabrication of Discs

As shown in Table II and Figure 4, large $^{239}PuO_2$-ZrO_2 discs have been fabricated in the 0.5 in. thickness. In addition, two large 0.25 in. thick $^{238}PuO_2$-ZrO_2 discs have been fabricated. Each disc has a power of 21 watts. The first attempt to press the $^{238}PuO_2$-ZrO_2 powders was only partially successful, and the unfired specimen had several edge defects. However, sintering this specimen showed that no detrimental effects were to be expected during the firing steps. After slight procedural changes, the second disc was pressed and sintered to form a satisfactory product, as shown in Figure 14.

7. Additional SEPO/SNS Safety Requirements

A. Pellets for Arc Tunnel Tests: The samples that have been sent to Sandia Laboratories are listed in Table VIII.

B. Specimens for Impact Tests: The samples that have been sent to Sandia Laboratories for impact testing are shown in Table VIII. In addition, two large $^{239}PuO_2$-ZrO_2 discs were in storage at LASL on October 18 for these tests.

C. Unspecified Tests: As shown in Table II, numerous pellets, discs, and powders are available for test.

III. FUNDAMENTAL STUDIES OF HELIUM RELEASE

A. Transmission electron microscopy:

Thin films of five actinide oxides have been examined by transmission electron microscopy during and after in situ annealing. Specimens have been prepared in three ways: by vacuum deposition of all five oxides onto copper substrates; by cleaving polycrystalline air-fired bulk ThO_2 and PuO_2; and by oxidation of electrochemically thinned thorium metal and delta plutonium alloy. For purposes of this report only results from the deposition preparation method will be discussed. (Within the physical limitations of the sample type, however, all specimens behaved similarly.)

Films about 1000Å in thickness were prepared by evaporation of the oxide from a resistance heated tungsten basket onto an electro-polished copper target maintained at room temperature. The oxide was deposited at the rate of ~5Å/sec under a background pressure of ~10^{-5} Torr. The oxide films were floated off the copper substrates in a 30% by volume HNO_3 in CH_3CH_2OH

7

mixture, washed and mounted on grids.

As deposited, the oxides were randomly oriented and the grains were less than 100Å in diameter. Annealing, by use of an unapertured electron beam, caused growth of the grains to final diameters of $\sim 2\mu m$, with grain diameter to foil thickness ratios approximating 10:1 (Figure 15). Initial grain growth was found to occur at temperatures as low as 500°C for AmO_2, and 1000°C for UO_2; however, to obtain large grains in PuO_2, NpO_2 and ThO_2 temperatures between 1300 and 1500°C were required.

During annealing, the following features were observed in the films:

1) In ThO_2, NpO_2 and PuO_2 extensive microwinning was observed by electron diffraction as well as microscopy (Figure 16). This feature was universal in well-annealed grains of ThO_2 and NpO_2 and was frequently present in PuO_2. However, only an occasional twin was seen in UO_2, and none in AmO_2.

2) During preparation, 2 or more layers of the original frequently overlapped. Heating caused sintering together of these layers. Grains formed from such regions contained large numbers of cavities (Figure 17), but this feature was never observed in grains grown from single layers of evaporated foil. During annealing, the high temperature produced grooving at grain boundaries and triple points and when these grooves were trapped inside the single final layer formed by the sintering of the multiple thicknesses cavities were the result. This feature appeared in all five of the oxides although in UO_2 and AmO_2 they were less distinctly geometric (Figure 18) and in both these oxides they annealed out easily upon further heating.

3) The edges of fully annealed grains maintained distinctly geometric shapes (Figure 19). This effect was especially marked in ThO_2 and NpO_2, less so for PuO_2 and UO_2 (Figure 20), and was almost absent in AmO_2.

4) Another aspect of the sintering behavior was the tendency for cracks in the film to bridge and heal themselves by growth of grains from the edges of the crack (Figure 21). This effect was most common in the AmO_2, UO_2 and PuO_2. For NpO_2 and ThO_2 the process rarely completed the healing of the crack. However, when bridged, subsequent grain growth obliterated all trace of the original crack in the final fully annealed structure.

Electron diffraction was used to index a large number of grains of ThO_2 and PuO_2. The results are listed in Table IX.

Microtwins usually were found to be parallel to the $<110>$ or $<135>$. These two orientations were also common for the edges of the cavities and the geometric edges of the annealed foils.

The distinctness and heat stability of the three features observed (microtwin, cavities and edges) were greatest for ThO_2 and NpO_2. In PuO_2 the cavities were often rounded and material surface diffusion greater (bridging of cracks). In UO_2 and AmO_2 no twins were seen, the cavities filled in or annealed out easily and edges only suggested geometric forms. It is obvious that the relative melting points of those materials affect the observed features, but quantitative statements are not yet possible.

B. Helium bubble formation

An investigation is presently under way to determine the relation of helium bubble formation to structural defects in actinide metal oxides. Thus far, a device has been constructed to allow deposition of helium atoms (in the form of alpha particles) just beneath the surface of oxide samples, and metallographic procedures have been developed for examination of the resulting structures.

A schematic drawing of the alpha bombardment test chamber is shown in the accompanying Figure 22. Alpha particles are accelerated to 9 MeV in a tandem Van de Graaff accelerator, and enter the device at the right. As the beam proceeds to the left, it passes through a focusing aperture, a valve (to allow isolation of radioactive samples from the accelerator), another focusing aperture, and a 1/2-mil Havar foil window, before reaching the target area. The Havar (a cobalt-iron-chromium-nickel alloy) serves the dual purpose of degrading the beam energy to the desired 5 MeV and of isolating radioactive samples. Beam divergence

8

problems require that the foil be kept close to the sample.

The movable aperture just in front of the target contains an aperture hole, a ZnS disk, and a quartz disk. The disks will luminesce when struck by the beam of alpha particles, and are present for alignment purposes. After final beam alignment, the aperture hole is swung into place to allow the 1/8-in. dia. beam to strike the oxide target. A -300 V bias is applied to the aperture plate to control electron emission from the sample.

The oxide specimen is mounted on a water-cooled copper plate. The number of alpha particles deposited is determined by monitoring the electrons which flow to the sample (through the plate) to neutralize the helium ions.

An alpha particle deposition energy of 5 MeV was chosen because it duplicates the energy of alpha decay in plutonium, and because higher energies might lead to fission of the actinide atoms with resultant severe lattice damage. Calculations show that 5 MeV alpha particles will be deposited in a narrow band about 10 microns beneath the sample surface. As deposited, the helium will be present as individual atoms. Subsequent heating will cause agglomeration into helium bubbles, and these will be examined microscopically. Bubble behavior will be evaluated as a function of annealing temperature, annealing time, and will be correlated with crystal defects such as grain boundaries and voids.

Initial studies will be carried out on ThO_2, an essentially non-radioactive compound of fluorite structure. Special metallographic mounting and polishing procedures have been developed to allow examination of this ceramic at high magnification without difficulty from edge rounding. After bombardment and handling procedures have been worked out, studies will be made on $^{239}PuO_2$, which is similar in many ways to ThO_2.

C. X-ray line broadening analyses:

The changes in crystallite size and strain in the lattice of PuO_2 as a function of time of self-irradiation will be studied through the technique of x-ray line broadening analysis. Other items of interest that might be obtained from the x-ray examination are changes in lattice parameters, stacking fault probabilities, strains as a function of distance perpendicular to khl planes and twinning probabilities.

A material that has a large crystalline size and no lattice strain or other faults or defects will, in general, yield a quite sharp powder pattern line upon x-ray diffraction examination. A broadened x-ray line occurs when some physical operation changes the crystallite size from large to small and/or introduces large strains in the lattice. By comparing the broadened x-ray line with the sharp line through the use of a rather detailed mathematical procedure called "deconvolution" estimates of the small crystallite size and large strains can be made.

A computer program has been written to assist in the analysis of the data. Its general philosophy of operation and the evaluation of the results obtained will be described below. There are three methods used for the determination of crystallite size and strain; the obtaining of the integral breadth of the line profile, the examination of Fourier coefficients describing the shape of a line, and the evaluation of the second moment of the line profile about its centroid. All three methods are incorporated in the computer program.

REFERENCES

1. "Studies on the Formation of Pu_2O_3 in the Sintering of PuO_2," W. C. Pritchard and R. L. Nance, Los Alamos Scientific Laboratory Report No. LA-3493 (1966).

2. "Plutonium-Uranium Mixed Oxides," N. H. Brett, J. D. L. Harrison, and L. E. Russell, Plutonium 1960, p. 492, Cleaver-Hume Press, Ltd., London (1961).

3. "Compaction and Sintering of PuO_2-Mo Powder Mixtures," W. C. Pritchard, K. A. Johnson, J. A. Leary, and W. J. Maraman, Los Alamos Scientific Laboratory Report No. LA-2621 (1961).

4. "Preparation and Evaluation of Refined Plutonium-238," Document CMB-1458 (July 17, 1968) Annual Report for the Period July 1, 1967 - June 30, 1968, by Los Alamos Scientific Laboratory; Work Sponsored by the Division of Isotopes Development, U. S. A. E. C.

5. "Thermal Properties of Comositions in the System UO_2-ZrO_2-CaO," R. S. Kern and R. J. Beals, Ceram. Bull. **46**, 1154 (1967).

6. "Self-Irradiation Damage in Plutonium Ceramics," C. W. Bjorklund, R. M. Douglass, and J. A. Leary, Bull. Amer. Ceram. Soc. **46**, 901 (1967).

TABLES

Table I

GIBBS STANDARD FREE ENERGIES OF FORMATION
(kcal/g – atom of oxygen)

	$-\Delta G_T^o$	
	$1000^o K$	$2000^o K$
PuO_2	105	85
ZrO_2	108	86
ThO_2	124	102
CaO	127	98

Table III

Chemical Composition of Typical Powders

	Concentration, ppm by wt., or %			
Element	ZrO_2 |X|	ZrO_2 |Y|	ThO_2	PuO_2
Li	< 30		< 0.5	< 0.2
Be	< 1	< 1	< 0.5	< 0.1
B	< 3	< 3	0.5	3
Na	300	200	20	<10
Mg	500	50	2	<10
Al	0.4%	0.1%	20	15
Si	0.1%	0.5%	10	45
Ca	3	3	10	10
Ti	0.3	100		
V	< 10	50	< 100	
Cr	10	50	2	10
Mn	500	50	< 1	< 1
Fe	0.1%	400	20	20
Co	< 30	< 30	< 5	<10
Ni	100	10	< 2	< 5
Cu	30	30	2	5
Zn	< 30	< 30		<10
Nb	< 300	< 300		
Mo	< 100	< 100		
Sn	< 10	< 30		2
Hf	2%	2%		
Pb	< 30	< 30	2	< 1
Bi	< 10	< 3		< 1

Table II

LIST OF SPECIMENS PREPARED AS OF OCTOBER 20, 1968

Composition	Type	Number
$^{239}PuO_2 - ZrO_2$|Y|	Pellets	29
" "	Small discs	3
$^{239}PuO_2 - ZrO_2$|X|	Pellets	12
$^{239}PuO_2 - ThO_2$	Pellets	9
$^{239}PuO_2 - ZrO_2$|Y|	Large discs	4
$^{238}PuO_2 - ZrO_2$|Y|	Pellets	36
" "	Small discs	7
100% $^{238}PuO_2$	Pellets	14
$^{238}PuO_2 - ThO_2$	Pellets	12
$^{238}PuO_2 - ZrO_2$|Y|	Large discs	2
ZrO_2|Y|	Pellets	3
ThO_2	Pellets	3
	Total	137

Table IV

COMPATIBILITY TESTS IN PROGRESS AS OF OCTOBER 27, 1968
($900^o C$ TESTS)

Capsule	Alloy	Fuel Materials		
SCC-2	TZM	ZrO_2|X|,	$PuO_2 - ZrO_2$|X|,	PuO_2
SCC-3	"	"	"	"
			(1.7 watt/cc)	(4.4 watt/cc)
SCC-4	TZM	ZrO_2|Y|,	*PuO_2-ZrO_2|Y|,	*PuO_2-ZrO_2|Y|
SCC-5	"	"	"	"
			(1.7 watt/cc)	(3.5 watt/cc)
SCC-6	TZM	ThO_2,	PuO_2-ThO_2,	PuO_2
			(1.7 watt/cc)	(4.4 watt/cc)

* = ^{238}Pu, all others ^{239}Pu

CONFIDENTIAL
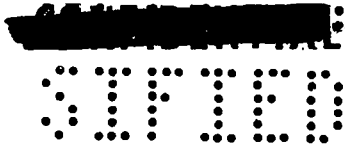
Table V

PELLETS IN STORAGE FOR He RELEASE MEASUREMENTS
(AS OF OCTOBER 20, 1968)

$^{238}PuO_2$	4.4 watts/cc
$^{238}PuO_2-ZrO_2$	3.5 watts/cc
$^{238}PuO_2-ZrO_2$	1.7 watts/cc
$^{238}PuO_2-ThO_2$	1.7 watts/cc

Table VI

THERMAL DIFFUSIVITY SAMPLES
(0.25 in. dia x 0.030 in. thick)

Composition	Number	Power Density
$^{238}PuO_2-ZrO_2$	2	1.7 watts/cc
$^{238}PuO_2-ZrO_2$	2	3.5 watts/cc

Table VII

$^{238}PuO_2-ZrO_2$ SAMPLES SHIPPED TO NRDL FOR SOLUBILITY TESTS
(0.25 in. dia x 0.25 in. tall)

Date Shipped	No. of Pellets	Power Density watts/cc
August 28	4, one with axial hole	4.4
September 24	4, " " " "	1.6
October 9	4, " " " "	3.5
October 15	4, " " " "	1.7

Table VIII

SAMPLES SENT TO SANDIA LABORATORIES

Type Test	No. of Specimens	Material	Type
Small tunnel[1]	3	$PuO_2 - ZrO_2$|X| (1.7 watt/cc)	standard
Small tunnel	3	$PuO_2 - ZrO_2$|X| (2.2 watt/cc)	standard
Small tunnel	4	ZrO_2|Y|	standard
Large tunnel[2]	2	"	spinning
Large tunnel	2	"	edge-on
Large tunnel	2	"	face-on
Large tunnel	10	ZrO_2|Y|	spinning
Impact[2]	2	"	face-on
Small tunnel	2	"	standard
	30		

Notes: (1) standard specimen for small tunnel test:
0.25 in. dia x 0.35 in. long; axial hole 0.060 in. dia x 0.080 in. deep

(2) standard specimen for large tunnel test and for impact:
2 in. dia x 0.5 in. thick
(spinning type has 3/16 in. dia diametral hole through)
(edge-on type has 1/4 in. dia blind diametral hole)
(face-on and impact types have no holes)

Table IX

FREQUENCY OF GRAIN ORIENTATION

Orientation			Number ThO_2 Grains	Number PuO_2 Grains
{211}			25	26
{111}			16	9
{110}			12	10
{123}			10	6
{233}			4	13
{334}			2	2
{100}			–	2
{223}	{127}	{120}		
{116}	{310}	{152}	–	1 each
{115}	{318}			

11

SOLID SOLUTION FUEL FLOWSHEET

```
┌─────────────┐         ┌─────────────┐         ┌─────────────┐
│    Weigh    │────────▶│    Blend    │◀────────│    Weigh    │
│             │         │   Powders   │         │             │
└─────────────┘         └─────────────┘         └─────────────┘
       ▲                       │                       ▲
       │                       ▼                       │
┌─────────────┐         ┌─────────────┐         ┌─────────────┐
│Grind to -325│         │    Weigh    │         │Grind to -325│
│    Mesh     │         │             │         │    Mesh     │
│(U.S. Std.   │         └─────────────┘         │(U.S. Std.   │
│   Sieve)    │                │                │   Sieve)    │
└─────────────┘                ▼                └─────────────┘
       ▲                ┌─────────────┐                ▲
       │                │ Cold Press  │                │
┌─────────────┐         └─────────────┘         ┌─────────────┐
│ As Received │                │                │ As Received │
│ 238PuO2     │                ▼                │ MO2 Powder  │
│ Powder      │         ┌─────────────┐         │             │
└─────────────┘         │   Sinter    │         └─────────────┘
                        └─────────────┘
                               │
                               ▼
                        ┌─────────────┐
                        │   Inspect   │
                        └─────────────┘
```
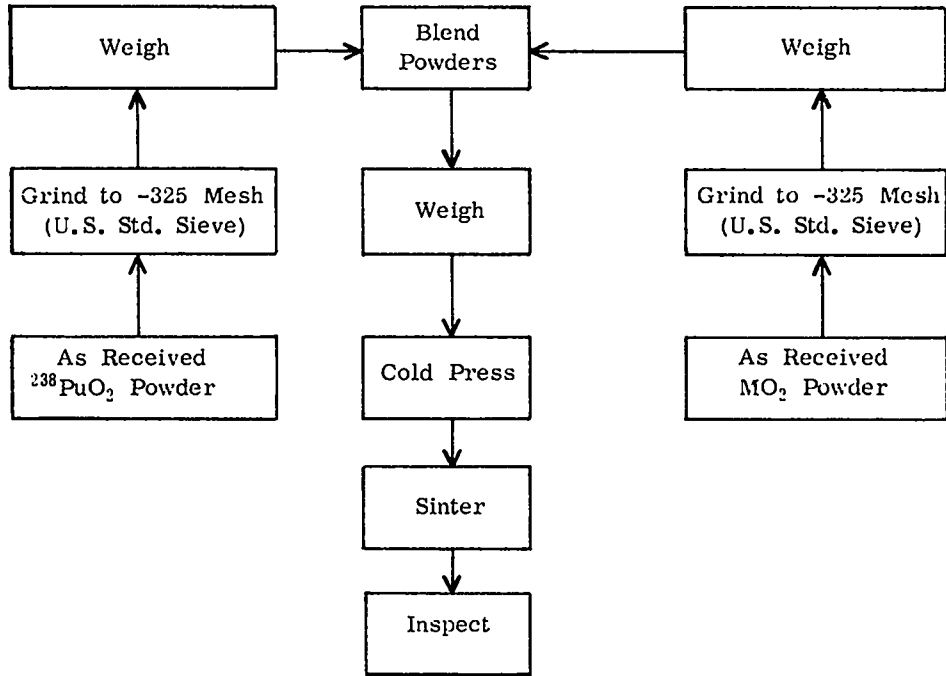
Figure 1

Figure 2. $^{239}PuO_2$-ZrO_2 pellets, 0.25 in. dia x 0.25 in. tall
(39 m/o PuO_2, 1.7 watts/cc conc.)

Figure 3. PuO$_2$-ZrO$_2$ solid solution developmental discs (0.25 in. dia, 0.027 in., 0.039 in., and 0.050 in. thick), on top of metal columns. Scale markings are 1/64 in. each.
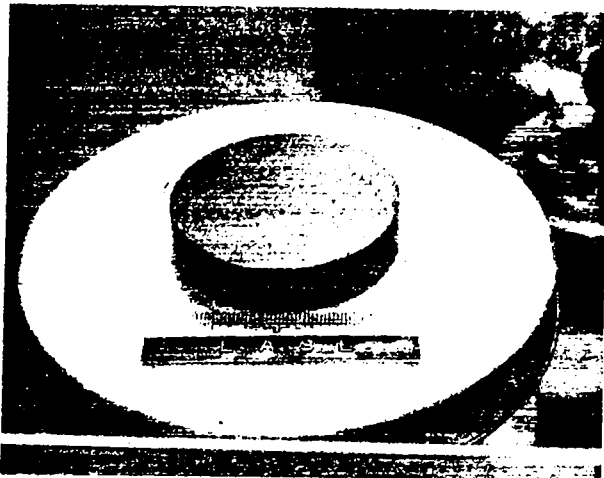
Figure 4. Large ^{239}PuO$_2$-ZrO$_2$ solid solution disc (39 m/o PuO$_2$, 2 in. dia x 0.5 in. tall)

LATTICE PARAMETERS OF PuO$_2$ SOLID SOLUTIONS AS A FUNCTION OF COMPOSITION

PuO$_2$ - ThO$_2$

PuO$_2$ - CeO$_2$

PuO$_2$ - ZrO$_2$ (CARROLL)

PuO$_2$ - ZrO$_2$ |CaO|

LATTICE PARAMETER, Å

MOLE PERCENT PuO$_2$
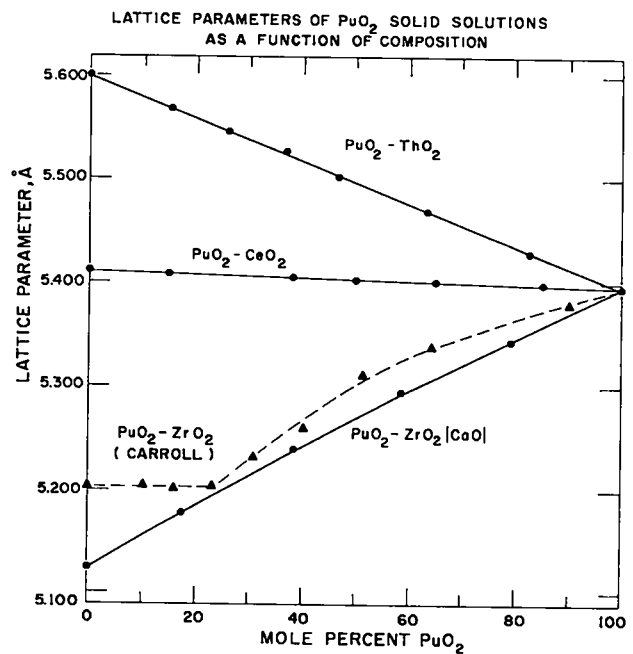
Figure 5

^{239}PuO$_2$ (11.1 g/cc)
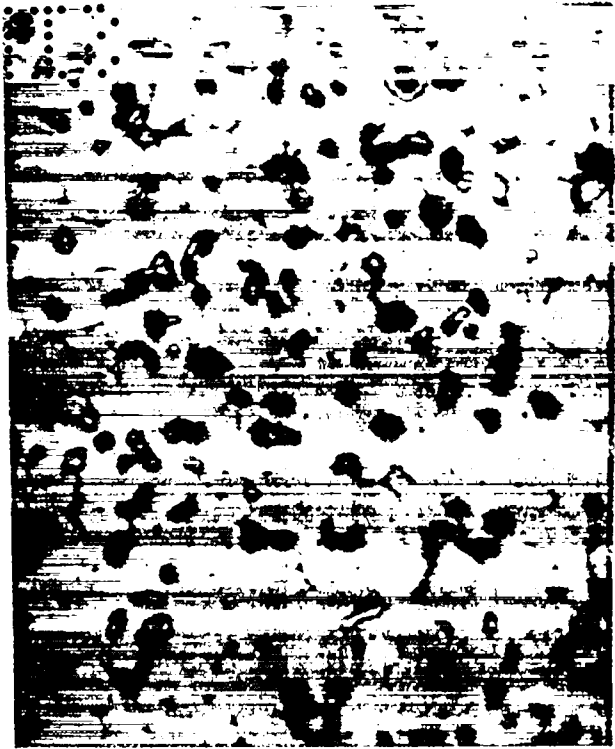
As Polished
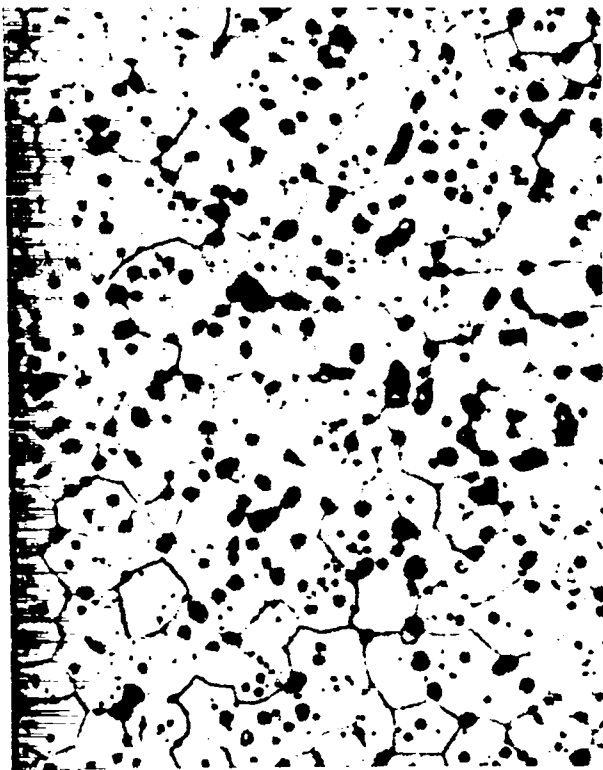
^{238}PuO$_2$ (10.2 g/cc)
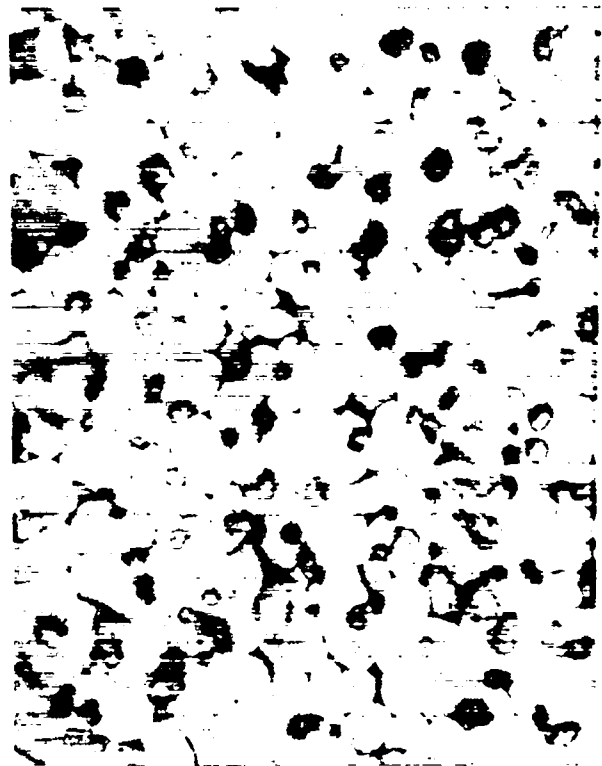
Hot Acid Etch
(HCl, HBr, HF)

Figure 6. Microstructures of PuO$_2$ specimens,
500X (dark areas are pores)

Figure 7. Microstructure of PuO$_2$-ZrO$_2$ solid solution,
500X (7.04 g/cc, 39 m/o PuO$_2$, gray areas
are high in Fe, Al, and Si)

14
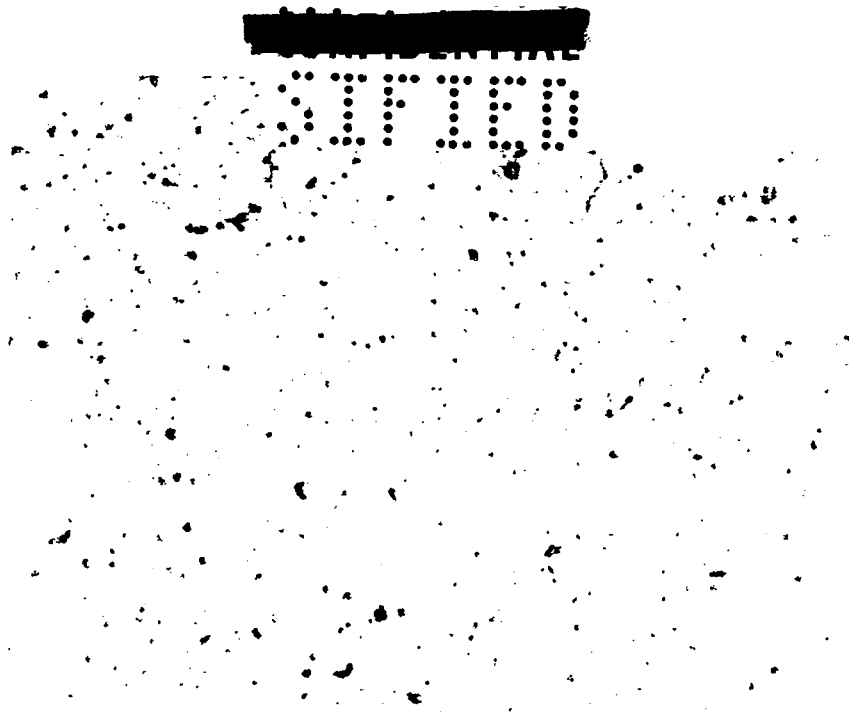
Figure 8. Microstructure of PuO_2-ThO_2 Solid Solution, 750X
(9.7 g/cc, 40 m/o PuO_2)

ALPHA PARTICLE AUTORADIOGRAPHS
PuO_2 AND PuO_2-ZrO_2|S|
(MAGNIFICATION: 14 X)
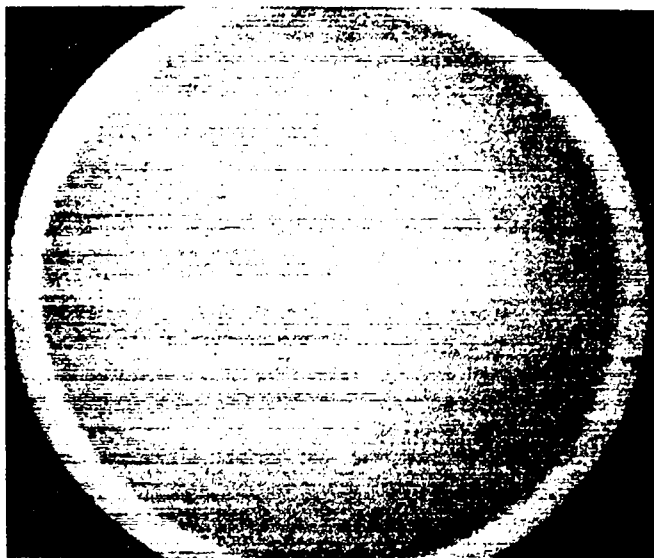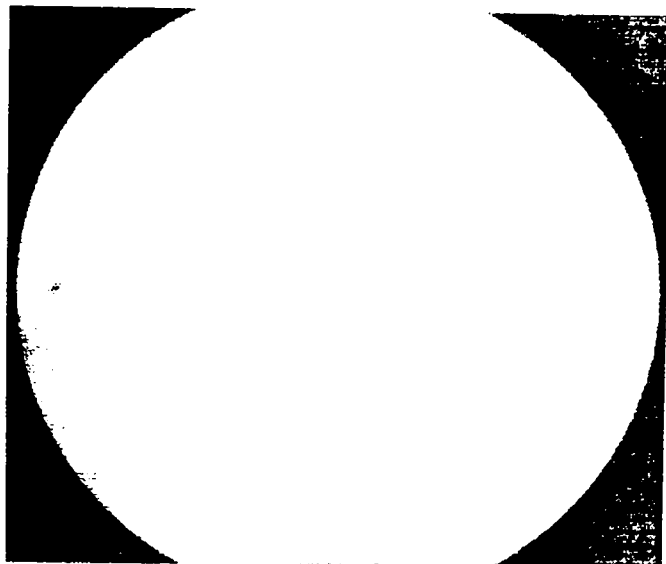
4.4 WATTS/cc	1.7 WATTS/cc
100% PuO_2	39 m/o PuO_2
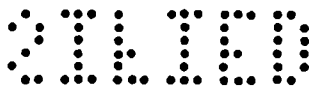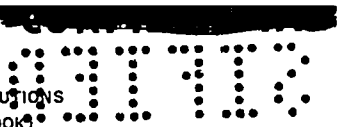
Figure 9

MELTING TEMPERATURES OF PuO_2 SOLID SOLUTIONS
(CURVES FROM PLUTONIUM HANDBOOK)

Figure 10

PuO_2-ThO_2

LIQUIDUS

SOLIDUS

STABILIZED

$PuO_2 ZrO_2$ (UNSTABILIZED)
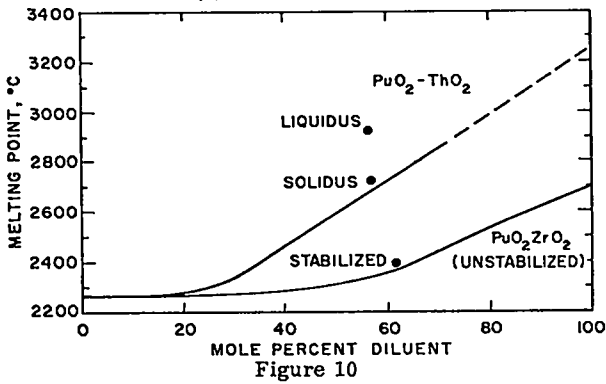
TYPICAL SOLID SOLUTION COMPATIBILITY
CAPSULE FOR TEST AT 900° C

SCALE : 2 = 1

WELD

HELIUM - ARGON
ATMOSPHERE

SPRING

INCONEL TUBE

TZM WEIGHT

TZM

PuO_2

TZM

$PuO_2 \cdot MO_2$ S.S.

TZM

MOLYBDENUM
INNER LINER

MO_2 DILUENT

Figure 11

TZM
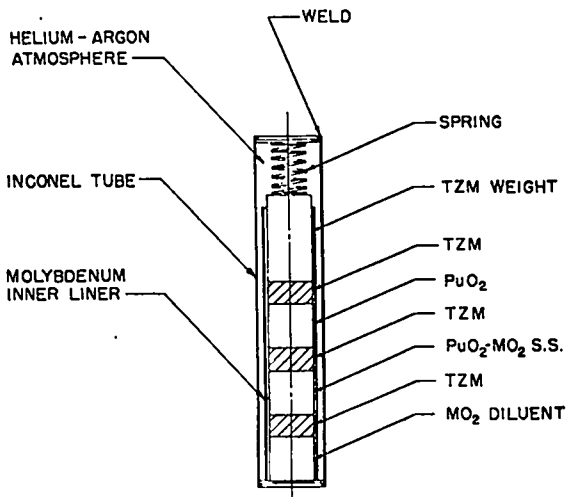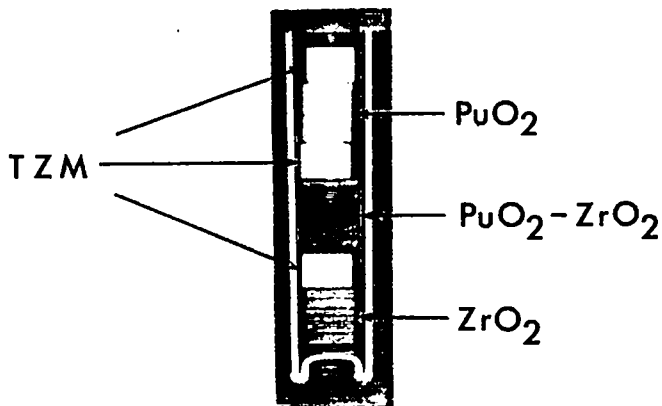
PuO_2

$PuO_2 - ZrO_2$

ZrO_2

Figure 12. Compatibility test capsule SCC-2 sectioned
after testing. 1.5X
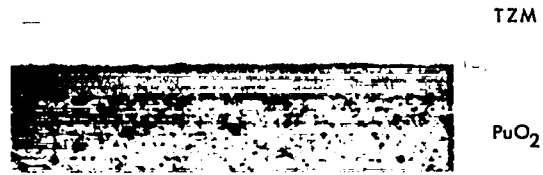
TZM

PuO_2

TZM

PuO_2-ZrO_2
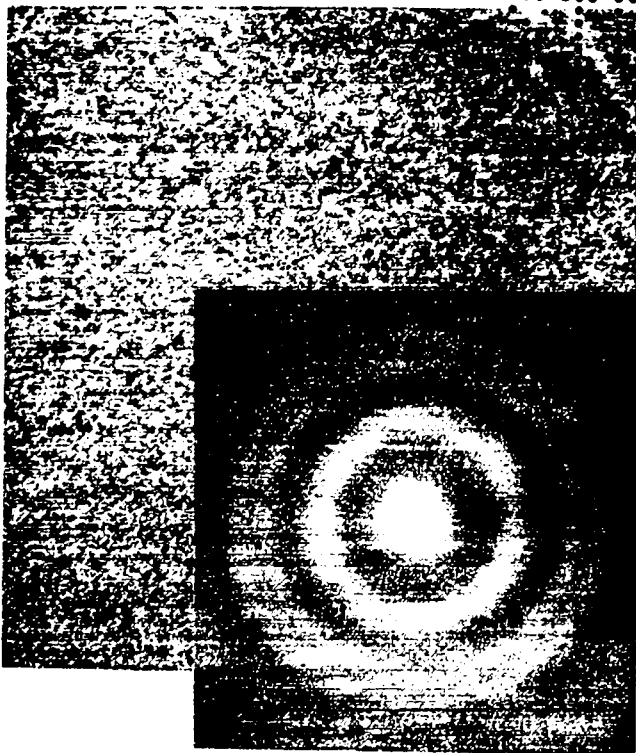
TZM

ZrO_2

Figure 13. TZM-ceramic interfaces, SCC-2
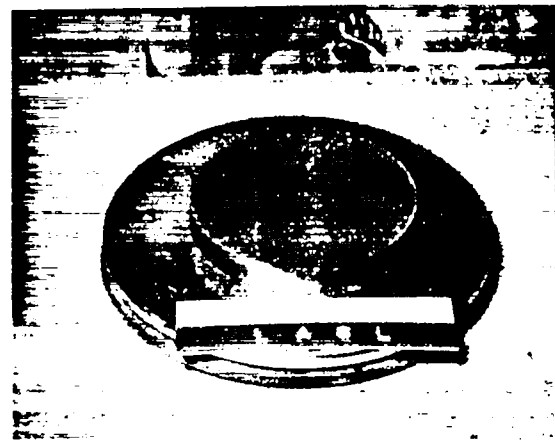
Figure 14. Large $^{238}PuO_2-ZrO_2$ solid solution disc
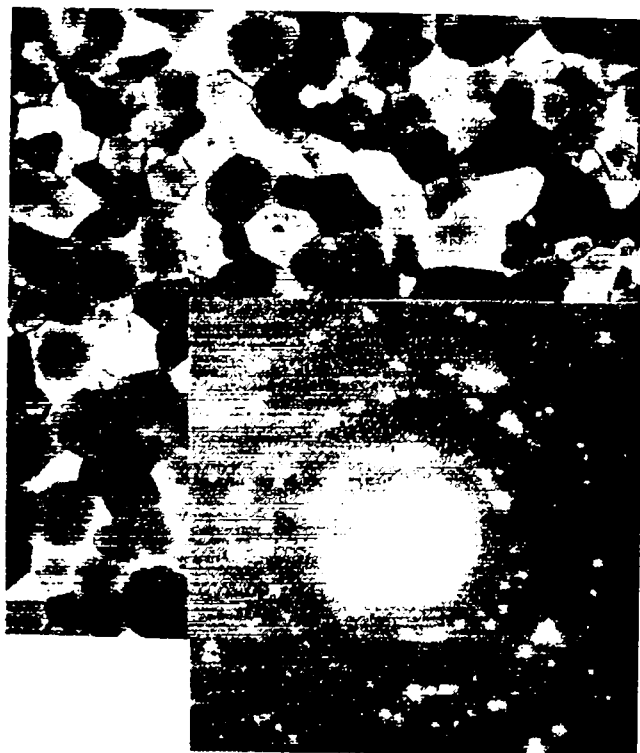(39 m/o PuO_2, 2 in. dia x 0.25 in. thick)
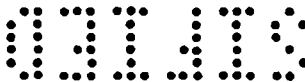
(a) As-deposited ThO$_2$

Figure 16. Fully annealed grain PuO$_2$ showing microtwins (55,000X)

(b) Early grain growth in PuO$_2$

Figure 15. Typical appearance of as-deposited and partially annealed actinide oxide foils together with their diffraction patterns (40,000X)

Figure 17. Geometric cavities in NpO_2. (50,000X)

Figure 18. Geometric cavities in UO_2. (62,000X)

Figure 19. Geometric edges of annealed ThO_2.
(72,000X)

Figure 20. Edges of annealed UO_2.
(50,000X)

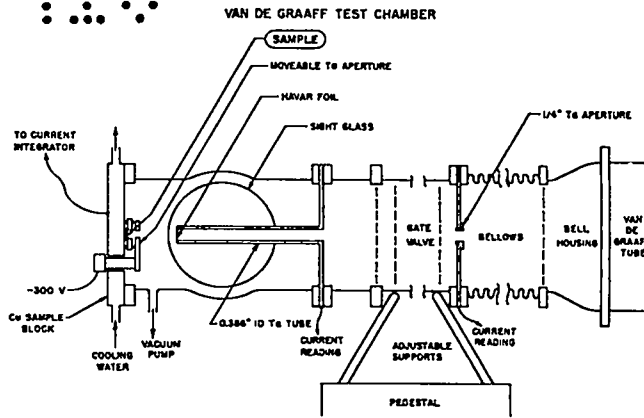Figure 21. Crack healing in PuO$_2$ evaporated films (78,000X)
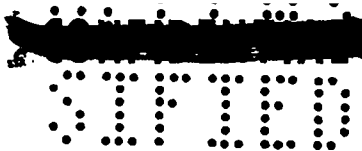

Figure 22

APPENDIX

PLUTONIUM DIOXIDE-ZIRCONIUM DIOXIDE SOLID SOLUTION DATA SHEETS

1. **Composition**

   PuO_2 and CaO stabilized ZrO_2* form a continuous series of solid solutions. Therefore the composition can vary from 0 to 100% PuO_2 depending on the power density required.

2. **Specific Power**

   PuO_2-ZrO_2 solid solutions can be varied from 0 to 0.402 w/g.

3. **Power Density**

   The power density is a function of ^{238}Pu concentration which in turn is a function of ZrO_2 concentration and porosity, as shown in Figure A1.

4. **Physical Properties**: Since very little has been measured on the solid solutions, most of the properties have been estimated using the reported properties for PuO_2 and ZrO_2.

---

* "ZrO_2" in these data sheets refer to ZrO_2 - 4.8 w/o CaO

a. Density (measured by x-ray diffraction). See Figure A1.

b. Average Linear Thermal Expansion Coefficient*
   $10.8 \times 10^{-6}/^{\circ}C$ (298-1273°K)

c. Heat Capacity. See Table AI

d. Enthalpy. See Table AI

e. Temperature of Phase Transformation

100 m/o PuO_2	melting point	2400°C(pure PuO_2 in sealed capsule)
40 m/o PuO_2 - 60 m/o ZrO_2		2400°C(in argon atmosphere)

No other phase transformations below the melting point were observed.

f. Latent Heat of Melting*

100 m/o PuO_2	16.8 kcal/mole
80 m/o PuO_2 - 20 m/o ZrO_2	17.6
40 m/o PuO_2 - 60 m/o ZrO_2	19.2
100 m/o ZrO_2	20.8

g. Vapor Pressures

At temperature of 2300°K,

	Pure PuO_2 †	80 m/o PuO_2
PuO_2:	2.3×10^{-5}atm.	1.8×10^{-5}atm.
ZrO_2:	——	1.4×10^{-8}atm.

	40 m/o PuO_2	Pure ZrO_2
PuO_2:	0.9×10^{-5}atm.	——
ZrO_2:	4.2×10^{-8}atm.	7.0×10^{-8}atm.

PuO_2 pressure at 1400°K = 1.5×10^{-13} atm.
†Pressure for $PuO_{1.87}$ which is congruent composition

h. Thermal Conductivity (cal/(cm$^{\circ}$C sec), at 100% density) *

Temp.	80 m/o PuO_2 - 20 m/o ZrO_2
973°K (700°C)	7.9×10^{-3}
1473°K (1200°C)	6.4×10^{-3}

Temp.	40 m/o PuO_2 - 60 m/o ZrO_2
973°K (700°C)	5.7×10^{-3}
1473°K (1200°C)	3.3×10^{-3}

i. Thermal Diffusivity for Pressed and Sintered Pellets* (cm^2/sec, 95% density)

Temp.	80 m/o PuO_2 - 20 m/o ZrO_2
973°K (700°C)	9.0×10^{-3}
1473°K (1200°C)	7.2×10^{-3}
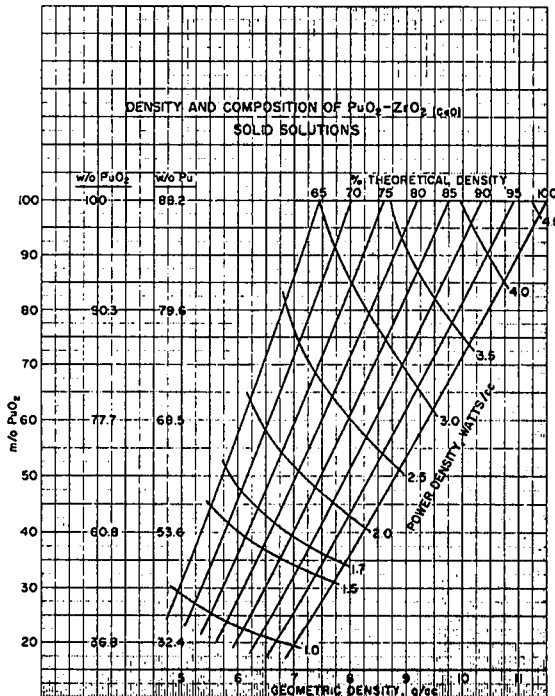
Figure A1
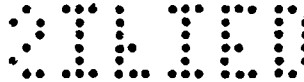
* Estimated
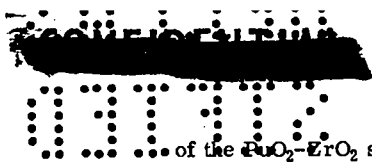
Table AI

Calculated Thermodynamic Functions for PuO_2-ZrO_2 Solid Solutions

Temp. $^\circ K$	C_p°	S_T°	$-\left(\dfrac{G_T^\circ - H_{298}^\circ}{T}\right)$	$(H_T^\circ - H_{298}^\circ)$	(ΔH_f°)	(ΔG_f°)
		cal mole⁻¹ deg⁻¹			kcal mole⁻¹	
298	....	19.2	19.2	0	-254.8	-242.2
800	21.0	42.0	29.0	11.7	-254.0	-218.4
1000	21.1	44.2	30.4	13.8	-254.0	-214.5
1200	21.4	45.1	33.0	18.1	-253.4	-206.6
1400	21.6	51.4	35.5	22.2	-252.4	-199.0
298	....	16.4	16.4	0	-258.6	-245.6
800	19.4	36.8	24.8	10.8	-257.6	-220.6
1000	19.6	38.8	26.0	12.8	-257.6	-215.5
1200	20.0	42.7	28.5	16.7	-257.4	-208.2
1400	20.3	45.5	30.6	20.8	-256.7	-200.3

Temp.	40 m/o PuO_2 – 60 m/o ZrO_2
973°K (700°C)	6.6×10^{-3}
1473°K (1200°C)	3.7×10^{-3}

j. Viscosity. Not available

k. Surface Tension. Not available

l. Spectral Emissivity. Not available

m. Crystallography

FCC Structure (fluorite)
Space Group Fm3m
Lattice Constant varies linearly from
100 m/o PuO_2 = 5.3954Å to 100 m/o ZrO_2=5.138Å

n. Solubilities

PuO_2–ZrO_2 solid solutions are more stable than PuO_2 itself (see Table AI). Therefore the solubility of the Pu from solid solutions would be expected to be lower than for PuO_2 itself.

o. Diffusion Rates. Not available

p. Selected Thermodynamics Functions are shown in Table AI.

5. Mechanical Properties[*]

a. Room Temperature Compressive Strength (psi)

80 m/o PuO_2 – 20 m/o ZrO_2	140,000
40 m/o PuO_2 – 60 m/o ZrO_2	220,000

b. Young's Modulus

22×10^6 psi decreasing as temperature increases

c. Shear Modulus

12×10^6 psi decreasing as temperature increases

6. Chemical Properties

Due to the larger negative free energy of formation

---

of the PuO_2-ZrO_2 solid solutions, the solid solutions should be less reactive towards metals by 3-5 kcal/mole depending on the composition and temperature.

SOURCES OF INFORMATION USED TO ESTIMATE PROPERTIES

1. N.H. Brett and L.E. Russell, _Plutonium 1960_, E. Grison, W.B.H. Lord, and R.D. Fowler, (ed), Cleaver-Hume Press, Ltd., London, 1961, p. 397.

2. K.K. Kelley, Bureau of Mines Bulletin 584, 1960, p. 209.

3. ANL-7438, 1968.

4. JANAF Thermochemical Tables, The Dow Chemical Co., Midland, Mich., 1964.

5. R.N.R. Mulford and L.E. Lamar, _Plutonium 1960_, E. Grison, W.B.H. Lord, and R.D. Fowler, (ed), Cleaver-Hume Press, London, 1961, 411.

6. W.A. Chupka, J. Berkowitz, and M.G. Inghram, The Journal of Chemical Physics 26, 1957, 1207.

7. R.S. Kern, R.J. Beals, Ceramic Bulletin 46, 1967, p. 1154.

PLUTONIUM DIOXIDE-THORIUM DIOXIDE SOLID SOLUTION DATA SHEETS

1. Composition

PuO_2 and ThO_2 form a continuous series of solid solutions. Therefore the composition can vary from 0 to 100% PuO_2 depending on the power density required.

2. Specific Power

PuO_2-ThO_2 solid solutions can be varied from 0 to 0.402 w/g.

3. Power Density

The power density is a function of ^{238}Pu concentration which in turn is a function of ThO_2 concentration and porosity as shown in Figure A2.
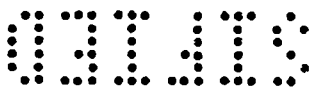
4. Physical Properties: Since very little has been measured, most of the properties have been estimated using the properties known for PuO_2 and ThO_2.
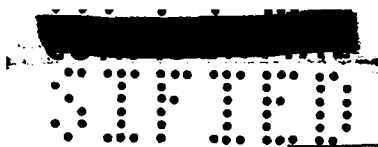
a. Density (measured by x-ray diffraction). See Figure A2.

b. Average Linear Thermal Expansion Coefficient[*]

$10.5 \times 10^{-6}/^\circ C$ (298-1273°K)

---

*Estimated

22

c. Heat Capacity. See Table AII

d. Enthalpy. See Table AII

e. Temperature of Phase Transformation, $^{\circ}$C

100 m/o PuO$_2$ melting point 2400°(pure PuO$_2$ in sealed capsule)

80 m/o PuO$_2$ - 20 m/o ThO$_2$ 2400°(open system)

40 m/o PuO$_2$ - 60 m/o ThO$_2$ 2925°(open system)

100 m/o ThO$_2$ 3300°

f. Latent Heat of Melting*

100 m/o PuO$_2$ 16.8 kcal/mole

80 m/o - 20 m/o ThO$_2$ 17.0

40 m/o - 60 m/o ThO$_2$ 17.5

100 m/o ThO$_2$ 18.0

g. Vapor Pressures (2300°K)

	Pure PuO$_2$†	80 m/o PuO$_2$*
PuO$_2$:	2.3 x 10^{-5} atm.	1.8 X 10^{-5}
ThO$_2$:	—	2 x 10^{-8}

	40 m/o PuO$_2$*	Pure ThO$_2$
PuO$_2$:	0.9 x 10^{-5}	
ThO$_2$:	7 x 10^{-8}	1.1 X 10^{-7}

† Pressure for PuO$_{1.87}$ (the congruent composition)
PuO$_2$ pressure at 1400°C = 1.5 x 10^{-13} atm.

h. Thermal Conductivity (100% density)*

700°C   9 x 10^{-3} cal/cm -$^{\circ}$C-sec

1200°C   6 x 10^{-3} cal/cm-$^{\circ}$C-sec

i. Thermal Diffusivity for Pressed and Sintered Pellets*

700°C   11 x 10^{-3} cm^2/sec

1200°C   7 x 10^{-3} cm^2/sec

j. Viscosity. Not available

k. Surface Tension. Not available

l. Spectral Emissivity. Not available

m. Crystallography

FCC Structure (fluorite)
Space Group Fm3m
Lattice Constant varies linearly from
100 m/o PuO$_2$ = 5.3954Å to 100 m/o ThO$_2$ = 5.598Å

n. Solubilities

PuO$_2$-ThO$_2$ solid solutions are more stable than PuO$_2$ itself (see Table AII). Therefore the solubility of the Pu from solid solutions would be expected to be lower than for PuO$_2$ itself.

o. Diffusion Rates. Not available

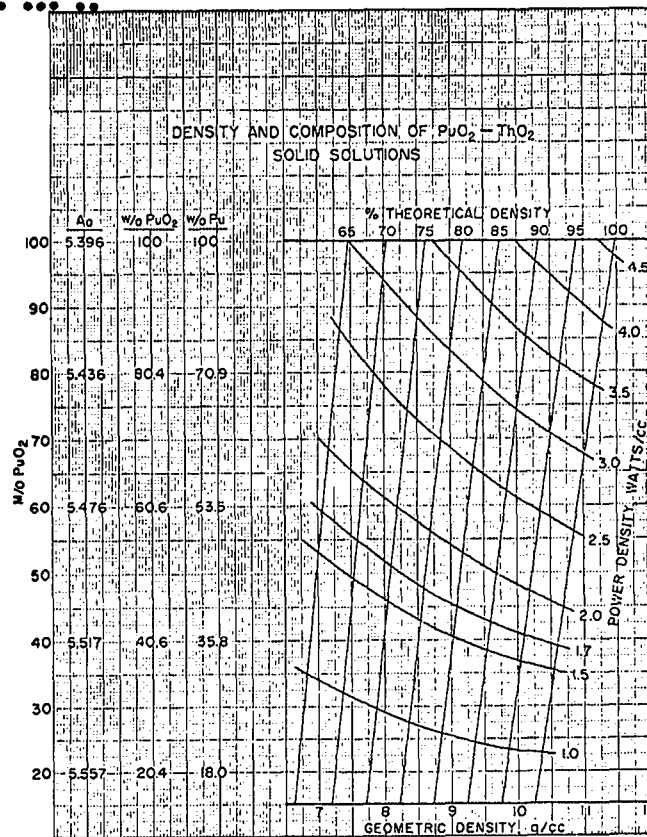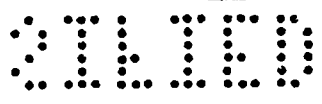p. Selected Thermodynamic Functions are shown in Table AII.

*Estimated

Figure A2

5. Mechanical Properties*

    a. Room Temperature Compressive Strength (psi)

        150,000

    b. Young's Modulus (psi)

        30×10^6

    c. Shear Modulus (psi)

        12×10^6

6. Chemical Properties

    Due to the larger negative free energy of formation of the PuO_2-ThO_2 solid solutions, the solid solutions should be less reactive towards metals by 10-20 kcal/mole depending on the composition and temperature.

SOURCES OF INFORMATION USED TO ESTIMATE PROPERTIES

1. R.N.R. Mulford and F.H. Ellinger, J. Phys. Chem. 62 (1958) 1466.

2. N.H. Brett and L.E. Russell, Plutonium 1960, E. Grison, W.B.H. Lord, and R.D. Fowler, (ed), Cleaver-Hume Press, Ltd., London (1961) 397.

3. B. Ohnysty and F.K. Rose, J. Am. Ceram. Soc. 47 (1964) 398.

4. ANL-7438, 1968.

5. A.C. Victor and T.B. Douglas, J. Res. Nat. Bur. Stds. 65 (1961) 105.

6. R.N.R. Mulford and L.E. Lamar, Plutonium 1960, E. Grison, W.B.H. Lord, and R.D. Fowler, (ed), Cleaver-Hume Press, Ltd., London (1961) 411.

7. R.J. Ackermann, E.G. Rauh, and R.J. Thorn, J. Phys. Chem. 67 (1963) 762.

8. JANAF Thermochemical Tables.

9. D.R. Stull and G.C. Sinke, "Thermodynamic Properties of the Elements," No. 18 in Advances in Chemistry Series, American Chemical Society, Washington D.C. (1956).

---

* Estimated

24

UNCLASSIFIED

UNCLASSIFIED